MODELING A MILLIMETER WAVE IMAGING SYSTEM WITH A 2.5D BICGS-FFT VOLUME INTEGRAL EQUATION TECHNIQUE

S. Van den Bulcke[1], A. Franchois[1], L. Zhang[2], and J. Stiens[2]

[1]*Department of Information Technology (INTEC-IMEC), Ghent University, 9000 Gent, Belgium, Email: sara.vandenbulcke@ugent.be, ann.franchois@ugent.be*
[2]*Department of Electronics and Informatics (ETRO), Vrije Universiteit Brussel, 1050 Brussel, Belgium, Email: lzhang@etro.vub.ac.be, jstiens@etro.vub.ac.be*

ABSTRACT

The imaging performance of an active mm-wave imaging system can be studied using accurate numerical electromagnetic simulations. We present an exact forward solver to calculate the three-dimensional (3D) scattered fields of a two-dimensional (2D) inhomogeneous dielectric object which is illuminated with a given 3D time-harmonic incident field. Since the size of the scattering objects can be very large with respect to the wavelength, a 2.5D configuration is adopted. This reduces the computational cost while it maintains the capability of accurately studying the system performance. The 3D scattered fields are calculated by discretizing a contrast source integral equation with the Method of Moments. The resulting linear system is solved iteratively with a stabilized biconjugate gradient Fast Fourier Transform method.

Key words: Forward solver; millimeter waves; volume integral equation technique.

1. INTRODUCTION

There are two different techniques for active millimeter wave imaging. The optical approach gives rise to a system which uses lenses for beam and image formation. These lenses produce artifacts in the image that can be reduced by using non-coherent illumination and averaging the obtained images. This method is a qualitative technique. Another imaging mode is a quantitative technique, which is derived from microwave imaging principles and is largely based on the exact solution of Maxwell's equations.
In both cases, an exact model of the wave-field propagation and scattering is indispensable to carefully study system performance and imaging capabilities. Therefore we developed an exact forward solver for two-dimensional (2D) inhomogeneous dielectric objects embedded in a homogeneous background medium.
The objects are illuminated with a given three-dimensional (3D) time-harmonic incident field and the 3D scattered field is computed. This 2.5D configuration is adopted since it reduces the computational burden while maintaining the capability of accurately studying the system performance. A volume integral equation approach is used, whereby a contrast source integral equation is discretized with the Method of Moments (MoM) and solved iteratively with a stabilized biconjugate gradient Fast Fourier Transform (BiCGS-FFT) method. The formulation of the algorithm is given in section 2 and comparisons of simulation results to analytic solutions for TE and TM polarizations and to measurements are presented in section 3.

2. FORMULATION

The 2.5D solver presented in this paper is an extension of the 2D-TE CG-FFT forward solver developed by [1].
The problem is formulated in the frequency domain and the time dependence $\exp(-j\omega t)$ is omitted. We consider a 2D inhomogeneous dielectric object embedded in free space with complex permittivity

$$\epsilon(\mathbf{r}) = \epsilon_r(\mathbf{r})\epsilon_0 = \epsilon'(\mathbf{r}) + j\epsilon''(\mathbf{r}), \tag{1}$$

with $\epsilon'(\mathbf{r})$ and $\epsilon''(\mathbf{r})$ representing the real and imaginary part of $\epsilon(\mathbf{r})$ and $\mathbf{r} = (x, y)$ the position vector. The imaginary part of the relative complex permittivity $\epsilon_r(\mathbf{r})$ is given by $\epsilon_r''(\mathbf{r}) = \frac{\sigma}{\omega\epsilon_0}$, with ω the angular frequency, ϵ_0 the permittivity of vacuum and σ the electric conductivity. The object is illuminated with a 3D time-harmonic incident field

$$\mathbf{E}^i(\mathbf{r}, z) = [E_1^i(\mathbf{r}, z), E_2^i(\mathbf{r}, z), E_3^i(\mathbf{r}, z)] \tag{2}$$

and the resulting scattered field is defined as

$$\mathbf{E}^s(\mathbf{r}, z) = \mathbf{E}(\mathbf{r}, z) - \mathbf{E}^i(\mathbf{r}, z), \tag{3}$$

with $\mathbf{E}(\mathbf{r}, z)$ the total field.
The problem is formulated in terms of the unknown electric flux density

$$\mathbf{D}(\mathbf{r}, z) = [D_1(\mathbf{r}, z), D_2(\mathbf{r}, z), D_3(\mathbf{r}, z)]. \tag{4}$$

When $\mathbf{E}^i(\mathbf{r},z)$ is expanded as $\mathbf{E}^i(\mathbf{r},\beta)e^{j\beta z}$, the integral equation over the object domain S takes the following form

$$\begin{bmatrix} E_1^i(\mathbf{r},\beta) \\ E_2^i(\mathbf{r},\beta) \\ E_3^i(\mathbf{r},\beta) \end{bmatrix} = \frac{1}{\epsilon(\mathbf{r})} \begin{bmatrix} D_1(\mathbf{r},\beta) \\ D_2(\mathbf{r},\beta) \\ D_3(\mathbf{r},\beta) \end{bmatrix} - \begin{bmatrix} k_0^2 + \frac{\partial^2}{\partial x^2} & \frac{\partial^2}{\partial x \partial y} & j\beta\frac{\partial}{\partial x} \\ \frac{\partial^2}{\partial x \partial y} & k_0^2 + \frac{\partial^2}{\partial y^2} & j\beta\frac{\partial}{\partial y} \\ j\beta\frac{\partial}{\partial x} & j\beta\frac{\partial}{\partial y} & k_0^2 - \beta^2 \end{bmatrix} \begin{bmatrix} A_1(\mathbf{r},\beta) \\ A_2(\mathbf{r},\beta) \\ A_3(\mathbf{r},\beta) \end{bmatrix}, \tag{5}$$

where $k_0 = \omega\sqrt{\epsilon_0\mu_0}$. The vector potential $\mathbf{A}(\mathbf{r},\beta)$ can be calculated as

$$\mathbf{A}(\mathbf{r},\beta) = \mathcal{F}^{-1}\left[F[G(\mathbf{r},\beta)]\ \mathcal{F}[\chi(\mathbf{r})\frac{\mathbf{D}(\mathbf{r},\beta)}{\epsilon(\mathbf{r})}]\right] \tag{6}$$

with $\mathcal{F}$ the forward 2D spatial Fourier transform and $\mathcal{F}^{-1}$ the inverse 2D spatial Fourier transform.
The scalar 2D Green's function is given by

$$G(\mathbf{r},\beta) = \frac{j}{4}H_0^{(1)}(\sqrt{k_0^2-\beta^2}|\mathbf{r}|) \tag{7}$$

and the normalized contrast function $\chi(\mathbf{r})$ is defined as

$$\chi(\mathbf{r}) = \frac{\epsilon(\mathbf{r})-\epsilon_0}{\epsilon(\mathbf{r})}. \tag{8}$$

The β-dependence is assumed in the following.
The spatial coordinate $\mathbf{r}$ is discretized by means of a rectangular 2D grid with a cell size of Δ in both directions and with N cells in the x-direction and M cells in the y-direction. We introduce the following staggered grids for $n = 0 \ldots N$ and $m = 0 \ldots M$:

$$\mathbf{r}_{n,m}^{(0)} = (n\Delta, m\Delta) \tag{9a}$$

$$\mathbf{r}_{n,m}^{(1)} = ((n-\frac{1}{2})\Delta, m\Delta) \tag{9b}$$

$$\mathbf{r}_{n,m}^{(2)} = (n\Delta, (m-\frac{1}{2})\Delta) \tag{9c}$$

$$\mathbf{r}_{n,m}^{(3)} = ((n-\frac{1}{2})\Delta, (m-\frac{1}{2})\Delta). \tag{9d}$$

In each cell with center $\mathbf{r}_{n,m}^{(0)}$ the complex permittivity $\epsilon(\mathbf{r})$ is assumed constant. Vectorial testing functions

$$\Psi^{(p)}(\mathbf{r}_{n,m}^{(p)} - \mathbf{r}) = \psi^{(p)}(\mathbf{r}_{n,m}^{(p)} - \mathbf{r})\mathbf{u}^{(p)} \tag{10}$$

are introduced for $p = 1, 2, 3$. $\mathbf{u}^{(1)}$, $\mathbf{u}^{(2)}$ and $\mathbf{u}^{(3)}$ represent the unit vectors in the x, y and z-direction. Multiplication of Eq. 5 with these vectorial testing functions and integration over the object domain S yields:

$$\begin{aligned} \int_S \psi^{(p)}(\mathbf{r}_{n,m}^{(p)} - \mathbf{r})E_p^i(\mathbf{r})\mathrm{d}\mathbf{r} = & \int_S \psi^{(p)}(\mathbf{r}_{n,m}^{(p)} - \mathbf{r})\frac{D_p(\mathbf{r})}{\epsilon(\mathbf{r})}\mathrm{d}\mathbf{r} \\ & - k_0^2\int_S \psi^{(p)}(\mathbf{r}_{n,m}^{(p)} - \mathbf{r})A_p(\mathbf{r})\mathrm{d}\mathbf{r} \\ & + \int_S \partial_p\psi^{(p)}(\mathbf{r}_{n,m}^{(p)} - \mathbf{r})\nabla\cdot\mathbf{A}(\mathbf{r})\mathrm{d}\mathbf{r},\ p = 1,2 \end{aligned} \tag{11a}$$

$$\begin{aligned} \int_S \psi^{(3)}(\mathbf{r}_{n,m}^{(3)} - \mathbf{r})E_3^i(\mathbf{r})\mathrm{d}\mathbf{r} = & \int_S \psi^{(3)}(\mathbf{r}_{n,m}^{(3)} - \mathbf{r})\frac{D_3(\mathbf{r})}{\epsilon(\mathbf{r})}\mathrm{d}\mathbf{r} \\ & - k_0^2\int_S \psi^{(3)}(\mathbf{r}_{n,m}^{(3)} - \mathbf{r})A_3(\mathbf{r})\mathrm{d}\mathbf{r} \\ & - j\beta\int_S \psi^{(3)}(\mathbf{r}_{n,m}^{(3)} - \mathbf{r})\nabla\cdot\mathbf{A}(\mathbf{r})\mathrm{d}\mathbf{r} \end{aligned} \tag{11b}$$

In the derivation of these equations it was assumed that $\psi^{(p)}(\mathbf{r}_{n,m}^{(p)} - \mathbf{r}) = 0$ for $\mathbf{r} \in \partial S$. ∂_1 and ∂_2 represent the partial derivatives with respect to x and y. The electric flux density $\mathbf{D}(\mathbf{r})$, the incident field $\mathbf{E}^i(\mathbf{r})$ and the vector potential $\mathbf{A}(\mathbf{r})$ are expanded as:

$$D_p(\mathbf{r}) = \epsilon_0\sum_{k=1}^{N}\sum_{l=1}^{M} d_{p;k,l}\ \psi^{(p)}(\mathbf{r} - \mathbf{r}_{k,l}^{(p)}), \tag{12a}$$

$$E_p^i(\mathbf{r}) = \sum_{k=1}^{N}\sum_{l=1}^{M} e_{p;k,l}^i\ \psi^{(p)}(\mathbf{r} - \mathbf{r}_{k,l}^{(p)}), \tag{12b}$$

$$A_p(\mathbf{r}) = \sum_{k=1}^{N}\sum_{l=1}^{M} a_{p;k,l}\ \psi^{(p)}(\mathbf{r} - \mathbf{r}_{k,l}^{(p)}). \tag{12c}$$

When inserting Eq. 12 in Eq. 11 and carrying out the divergence operator as well as interchanging the order of integration and summation, the weak form of the integral equation is obtained for every $\mathbf{r}_{n,m}^{(p)} \in S$ ($p = 1, 2, 3$). The functions $\psi^{(p)}(\mathbf{r})$, $p = 1, 2, 3$ are defined as:

$$\psi^{(1)}(\mathbf{r}) = \Lambda(x; 2\Delta)\Pi(y; \Delta), \tag{13a}$$

$$\psi^{(2)}(\mathbf{r}) = \Pi(x; \Delta)\Lambda(y; 2\Delta), \tag{13b}$$

$$\psi^{(3)}(\mathbf{r}) = \Lambda(x; 2\Delta)\Lambda(y; 2\Delta), \tag{13c}$$

in which $\Lambda(x; 2\Delta)$ represents a one-dimensional triangle function in the x-direction of support 2Δ and $\Pi(y; \Delta)$ represents a one-dimensional pulse function in the y-direction of support Δ.
In Eq. 6 the field values of $\mathbf{D}(\mathbf{r})$ are replaced by the discrete values $d_{p;n,m}$ and 2D spatial discrete Fourier transforms are used. Therefore the Green's function is integrated over a circle with center $\mathbf{r}_{n,m}^{(0)}$ and radius $\frac{\Delta}{2}$. The resulting value is then divided by the surface of that circle:

$$g_{n,m} = \begin{cases} (\frac{j}{\Delta k_0})J_1(k_0\frac{\Delta}{2})H_0^{(1)}(k_0\Delta\sqrt{n^2+m^2}) \\ (\frac{j}{\Delta k_0})\left[H_1^{(1)}(k_0\frac{\Delta}{2}) + \frac{4j}{\pi\Delta k_0}\right] & n = m = 0. \end{cases} \tag{14}$$

This procedure gives no problem in handling the singularity of the Green's function at $\mathbf{r} = 0$ [2]. This leads to

$$a_{p;n,m} = \Delta^2 DFT^{-1}\left[DFT[g_{n,m}]DFT[\chi_{n,m}^{(p)}d_{p;n,m}]\right] \tag{15}$$

for $p = 1, 2, 3$ in which

$$\chi^{(1)}_{n,m} = \frac{1}{2}(\chi((n-1)\Delta, m\Delta) + \chi(n\Delta, m\Delta)), \quad (16a)$$

$$\chi^{(2)}_{n,m} = \frac{1}{2}(\chi(n\Delta, (m-1)\Delta) + \chi(n\Delta, m\Delta)), \quad (16b)$$

$$\chi^{(3)}_{n,m} = \frac{1}{4}(\chi((n-1)\Delta, (m-1)\Delta) + \chi((n-1)\Delta, m\Delta) + \chi(n\Delta x, (m-1)\Delta x) + \chi(n\Delta x, m\Delta x)). \quad (16c)$$

The system of Eqs. 11 and 15 is solved iteratively for the unknowns $d_{p;n,m}$ using a BiCGS-scheme ([3], [4]).

3. NUMERICAL AND EXPERIMENTAL RESULTS

3.1. Comparison to analytic solutions for TM and TE polarizations

In the simulations with our 2.5D BiCGS-FFT forward solver the initial estimate for d_p ($p = 1, 2, 3$) is chosen zero and the BiCGS iterations are stopped when the relative error drops below 10^{-8}. The object is a dielectric cylinder with relative permittivity $\epsilon_r = 2$ and with a radius equal to one wavelength ($\lambda_0 = 1$ mm, $f = 300$ GHz).

We first consider TM polarization. The incident field $E^i(\mathbf{r}) = E^i_3(\mathbf{r})$ ($\beta = 0$) is a line source at a distance of $10\lambda_0$ from the cylinder. The scattered fields $E^s_3(\mathbf{r})$ are calculated for 256 points on a circle with a radius of $10\lambda_0$ (Fig. 1 and Fig. 2). The simulation results are compared to the analytic solution and the normalized root mean square error (NRMSE) is determined:

$$error = \frac{\sqrt{\sum_{k=1}^{N} |E^s_{sim}(k) - E^s_{exact}(k)|^2}}{\sqrt{\sum_{k=1}^{N} |E^s_{exact}(k)|^2}} \quad (17)$$

where $N = 256$ denotes the number of detector points. Tab. 1 shows the different parameters of this simulation and Tab. 2 indicates that the error decreases as $O(\Delta)$.

Next, we consider TE polarization. The incident field $E^i(\mathbf{r}) = E^i_1(\mathbf{r})$ ($\beta = 0$) is a plane wave propagating in the y-direction, which is polarized along the x-direction. The scattered fields $E^s_1(\mathbf{r})$ and $E^s_2(\mathbf{r})$ are calculated in the same points as before (Fig. 3, Fig. 4, Fig. 5 and Fig. 6). The simulation results are again compared to the analytic solution and the NRMSE for $E^s_1(\mathbf{r})$ and $E^s_2(\mathbf{r})$ is indicated in Tab. 3. The error decreases as $O(\Delta^{1.3})$.

The differences between the numerical results and the analytic solution are due to the discretization and by consequence, the staircase approximation of the circle. Another inaccuracy lies in the averaging of the Green's function in (14) instead of an exact integration of the Green's function over each cell domain. Furthermore, the incident field is expanded in basis functions, multiplied by a testing function and then integrated over the object domain S ((11) and (12)). A more accurate result can be obtained if the integral over S of the incident field (not expanded), multiplied by the vectorial testing function, is calculated analytically.

Table 1. Parameters for TM and TE simulation

grid size	# unknowns	# it. TM	# it. TE
32x32	3072	47	34
64x64	12288	49	32
128x128	49152	51	30
256x256	196608	49	32
512x512	786432	51	38
1024x1024	3.145728e6	53	43
2048x2048	12.58291e6	54	41

Table 2. NRMSE for TM polarization

cells per λ	grid size	error E^s_3
10	32x32	0.4604
20	64x64	0.2369
40	128x128	0.1129
80	256x256	0.0587
100	512x512	0.0429
200	1024x1024	0.0225
500	2048x2048	0.0085

Table 3. NRMSE for TE polarization

cells per λ	grid size	error E^s_1	error E^s_2
10	32x32	0.1198	0.1063
20	64x64	0.0440	0.0385
40	128x128	0.0173	0.0163
80	256x256	0.0084	0.0084
100	512x512	0.0045	0.0039
200	1024x1024	0.0025	0.0022
500	2048x2048	0.00069	0.00055

3.2. Comparison to measurements

Fig. 7 represents the measurement setup used to validate our model. A W-band BWO (Backward Wave Oscillator) emits a 94GHz wave which is modulated by a lock-in amplifier with a 20 kHz signal and which is focused into a gaussian beam. The object is positioned along the beam axis to scatter the field. At the detecting side, an

open WR10 waveguide probe is used as the receiving antenna. To detect the received signal power, a W-band planar detector with a sensitivity of 550 mV/mW is applied. Its output voltage is fed back into the lock-in amplifier. A 30dB Faraday isolator is placed between the probe and the detector to eliminate the reflection from the planar detector side. The probe, isolator and detector are mounted together on a computer-controlled sled, which is able to move both parallel and perpendicular to the beam axis in a horizontal plane.

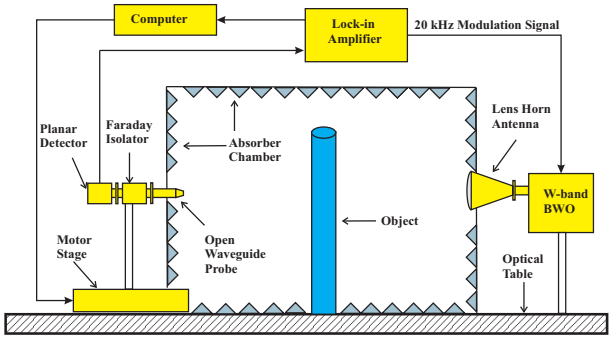

Figure 7. Schematic diagram of scattering measurement setup

The object is a metal cylinder with a diameter of 37.74 mm (which is about $11.5\lambda_0$, $f = 94$ GHz). In our model we choose $\epsilon_r' = 1$ and $\epsilon_r'' = 100$, which corresponds to $\sigma = 523$. No higher values for ϵ_r'' are chosen because the convergence of the BiCGS algorithm significantly slows down. The object is discretized using 10 cells per λ_0, yielding in a grid size of 256x256 cells. The incident field is a gaussian beam which illuminates the object completely. The distance between the source and the object is 45 cm. The total field amplitude is measured on a line of length 8 cm at a distance of 22.5 cm away from the center of the cylinder in 81 points, spaced 1 mm. Fig. 8 shows a comparison of a simulation with a measurement. There is a good agreement in the center of the line. At the edges the difference is probably due to the low value chosen for $\epsilon_r'' = 100$ in our model. In the future, measurements will be performed at the VUB with a millimeter wave vector network analyzer so that amplitude *and* phase can be measured and compared to simulations.

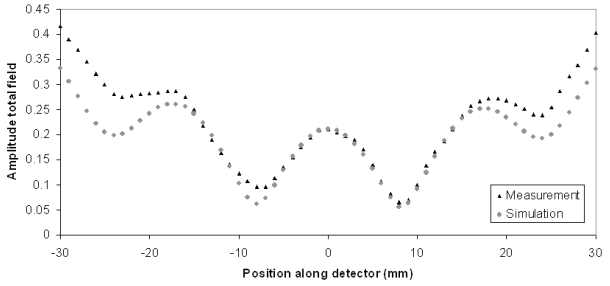

Figure 8. Amplitude of total field

4. CONCLUSIONS

A weak formulation of the BiCGS-FFT method for dielectric scatterers is presented. The simulated field curves are in very good agreement with the analytical solutions for TM and TE polarizations. A first comparison to measurements indicates that PEC materials are demanding test objects. More measurements will be done on various dielectric objects.
The convolution structure in the vector potential allows the application of FFT's, yielding a fast and efficient method for solving scattering problems.

ACKNOWLEDGMENTS

Research funded by a Ph.D. grant of the Institute for the Promotion of Innovation through Science and Technology in Flanders (IWT-Vlaanderen).

REFERENCES

[1] Zwamborn P. and van den Berg P.M., "A Weak Form of the Conjugate Gradient FFT Method for Two-Dimensional TE Scattering Problems", *IEEE Trans. on Microwave Theory and Techniques*, vol. 39(6), pp. 953-960, June 1991.

[2] Richmond J.H., "Scattering by a dielectric cylinder of arbitrary cross section", *IEEE Trans. on Antennas and Propagation*, vol. AP-13, pp. 334-341, May 1965.

[3] Xu X.M., Liu Q.H. and Zhang Z.Q., "The stabilized biconjugate gradient fast Fourier transform method for electromagnetic scattering", *J. Appl. Computat Electromag. Soc.*, vol. 17(1), pp. 97-103, March 2002.

[4] van der Vorst H.A., "BI-CGSTAB: A fast and smoothly converging variant of BI-CG for the solution of non symmetric systems", *SIAM J. Sci. Stat. Comput.*, vol. 13(2), pp. 631-644, 1992.

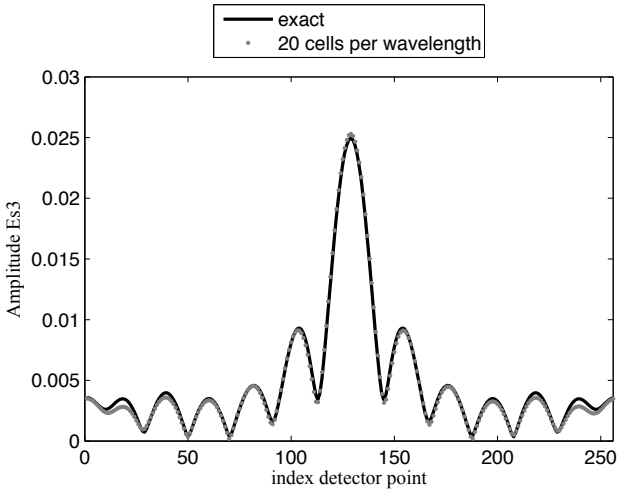

Figure 1. Amplitude of E_3^s for TM polarization

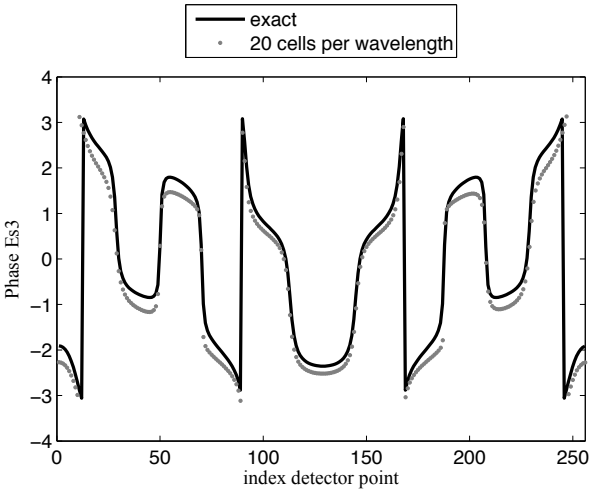

Figure 2. Phase of E_3^s for TM polarization

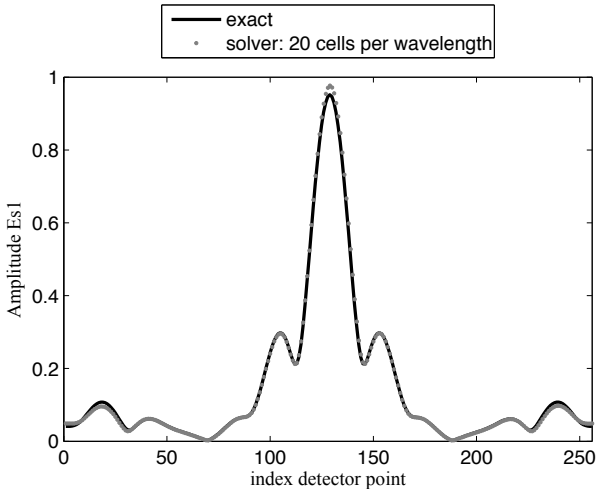

Figure 3. Amplitude of E_1^s for TE polarization

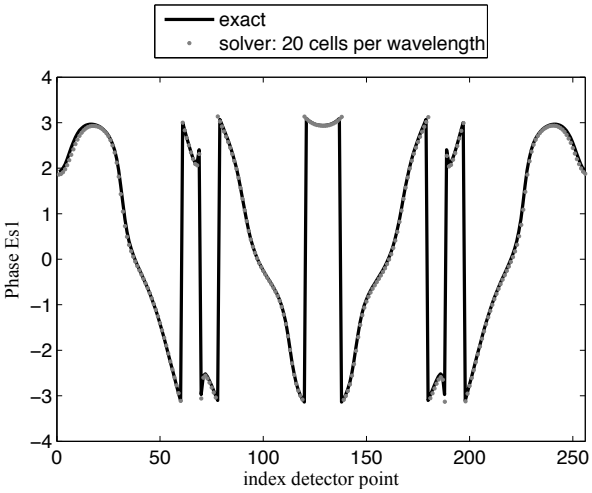

Figure 4. Phase of E_1^s for TE polarization

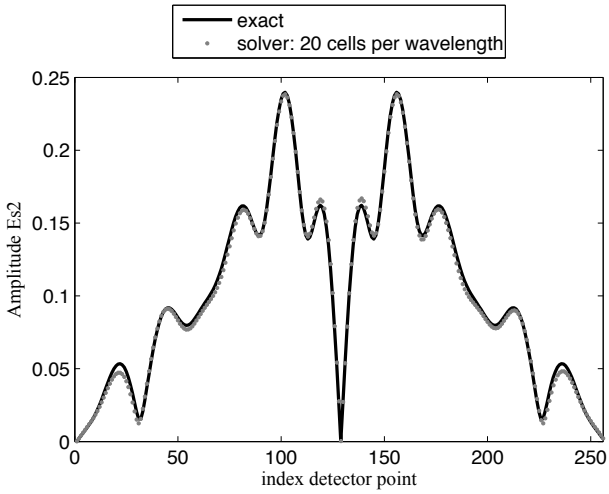

Figure 5. Amplitude of E_2^s for TE polarization

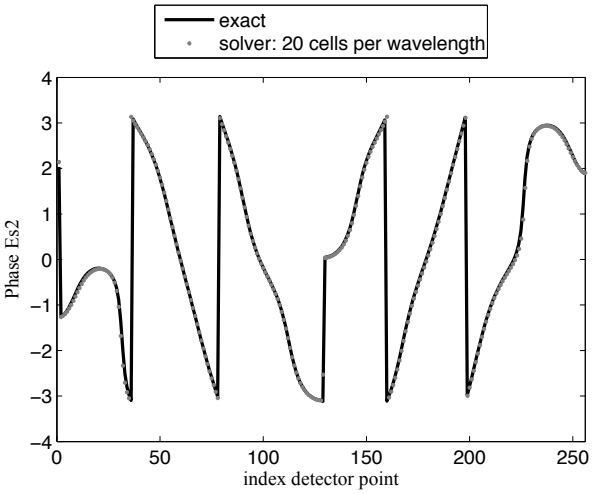

Figure 6. Phase of E_2^s for TE polarization

EuCAP 2006

esa

SP-626
Proceedings

ISBN 92-9092-937-5 ISSN 1609-042X

EUCAP CHAIRS

J. Mosig (General Chair), EPFL, CH
P. Ingvarson (Vice Chair), Saab Ericsson Space, S
B. Arbesser-Rastburg (Vice Chair), ESA-ESTEC, NL
A. Roederer (Honorary Chair), ESA-ESTEC, NL
P. Brachat (Local Chair), France Telecom R&D, F
C. Pichot (Local Chair), Univ. de Nice, F

Publication	Proceedings of the European Conference on Antennas and Propagation 'EuCap 2006', Nice, France (ESA SP-626, October 2006)
Editors	H. Lacoste & L. Ouwehand
Published by:	ESA Publications Division ESTEC Postbus 299 2200 AG Noordwijk The Netherlands
Printed in:	The Netherlands
Price:	60 Euros
ISBN No:	92-9092-9375
ISSN No:	1609-042X

SP-626
October 2006

Proceedings of

The European Conference on Antennas and Propagation: EuCAP 2006

6-10 November 2006
Nice, France

European Space Agency
Agence spatiale européenne